ARTICLE

Dosage-Controlled Intracellular Delivery Mediated by Acoustofluidics for Lab on a Chip Applications

Alinaghi Salari[ab]†, Sila Appak-Baskoy[ac]†, Imogen R. Coe[acd], John Abousawan[cd], Costin N. Antonescu[cd], Scott S.H. Tsai[ae]*, Michael C. Kolios[af]*
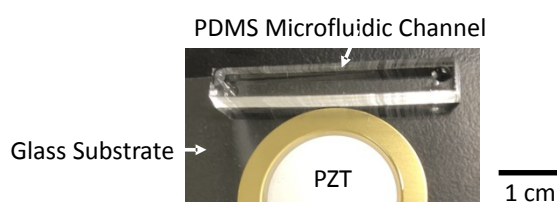
Figure S1. A photo of the acoustofluidic device.

Note S1. Image analysis protocol

To quantify the uptake, the fluorescence images of control and treated cells were taken using consistent levels of illumination and excitation-emission filters of 480/17-517/23 nm for green fluorescence imaging and 556/20-615/61 nm for red fluorescence imaging. For each experiment, we took the bright-field and fluorescence images of the same regions of interest (Figure S2a–b). Here, we assume the uptake is directly proportional to the fluorescence intensity of the cargo material.[1] To quantify the uptake, we use a semi-automated protocol, which consisted of five steps, as follows.

[a.] Institute for Biomedical Engineering, Science and Technology (iBEST), Toronto, ON M5B 1T8, Canada.
[b.] Biomedical Engineering Graduate Program, Ryerson University, Toronto, ON M5B 2K3, Canada.
[c.] Department of Chemistry and Biology, Ryerson University, Toronto, ON M5B 2K3, Canada
[d.] Molecular Science Graduate Program, Ryerson University, Toronto, ON M5B2K3, Canada
[e.] Department of Mechanical and Industrial Engineering, Ryerson University, Toronto, ON M5B 2K3, Canada
[f.] Department of Physics, Ryerson University, Toronto, ON M5B 2K3, Canada
† Equal contribution.
* Corresponding authors: Michael C. Kolios; Scott S.H. Tsai.
Electronic Supplementary Information (ESI) available: [details of any supplementary information available should be included here]. See DOI: 10.1039/x0xx00000x

- Step #1: First, we use ImageJ to select the areas covered by the cells on the bright-field image (Figure S2c).
- Step #2: Then, the selected area is copied to the fluorescence image (Figure S2d).
- Step #3: Next, the average fluorescence intensity of the selected area from the fluorescence image is calculated (i.e., $I_1 = \dfrac{Sum\ of\ the\ values\ of\ the\ pixels\ of\ the\ selected\ area}{Selected\ area}$).
- Step #4: Then, the average fluorescence intensity of the regions outside the selected area is calculated (i.e., $I_2 = \dfrac{Sum\ of\ the\ values\ of\ the\ pixels\ outside\ the\ selection}{Area\ outside\ the\ selection}$).
- Step #5: The final step is to calculate the difference of I_1 and I_2, which is considered as the average intensity of the delivered material to the cells (i.e., Mean Intensity = I_1- I_2).

To quantify the delivery efficiency, we take the control experiments as the reference for finding a fluorescence intensity threshold (I_t). This threshold is defined as an intensity that is higher than the mean intensity of 95% of the cell population in the control experiments [2,3]. In other words, only 5% of control cells exhibit fluorescence intensities higher than I_t. The delivery efficiency of each treatment is calculated as follows:

$$\text{Delivery efficiency (\%)} = \frac{Number\ of\ treated\ cells\ having\ a\ mean\ intensity\ above\ I_t}{Total\ number\ of\ treated\ cells} \times 100 \qquad (S1)$$

We note that, for the calculation of delivery efficiency in the gene delivery experiments, we considered the "Lipofection" groups (see Fig. S11a-b) as the control, in order to quantify our technique's improvement in delivery efficiency relative to the conventional transfection approach.
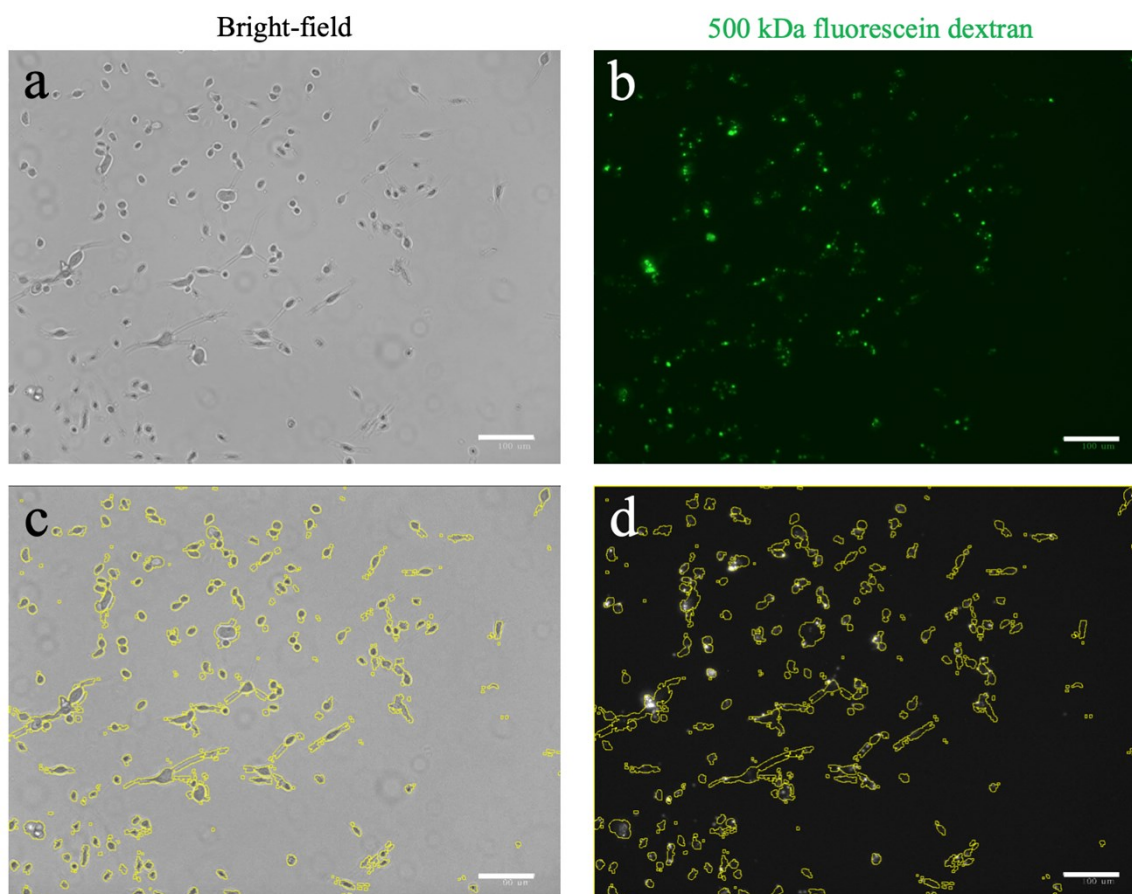
Figure S2. Sample (a) bright-field and (b) fluorescence images taken from the same regions of interest. (c) The outline of the cells on the bright-field image is selected using ImageJ. (d) The selected area is then transferred to the fluorescence image for further intensity calculations. The scale bars represent 100 μm.

Note S2. Shear stress calculations

For the calculation of shear stress imposed on the cells due to the microstreaming, we first measured the streaming velocity using 1 μm flow tracers. In our experiments, for the case of 1 W actuation power (which is the maximum power used in the continuous excitation experiments), the streaming flow near cells has a maximum velocity of $\sim 2 \frac{mm}{s}$, which is assumed to be equal to the velocity at the viscous boundary layer surrounding the cells. For a cell inside water with a viscosity of μ, this boundary layer can be estimated[4] to have a maximum thickness of $\delta \approx 2 \, \mu m$. At the boundary layer, assuming a Newton's law of viscosity, a shear stress of $\tau_c \approx 1 \, Pa$ will therefore be applied to the fluid outside the boundary layer, which can result in the formation of acoustic microstreaming. Based on the Newton's third law, we assume that a shear stress with an equal magnitude of τ_c is also exerted to the cell membrane (Figure S3).

We then expose the cells to similar shear stress with a flow-controlled system. To approximate the flow rate needed to inject the solution in the microfluidic channel for these continuous-flow experiments, we calculate the wall shear stress τ_w of a flow inside a microchannel and assume the cells will be exposed to

τ_w for the duration of experiments. For a microchannel that has a rectangular cross-section with an area of A, the average shear stress on the wall τ_w can be estimated as,[5] $\tau_w = \dfrac{4\pi^2 \mu u (1 + \varepsilon^2)}{3\sqrt{\varepsilon}(1 + \varepsilon)2\sqrt{A}}$, where, ε is the aspect ratio of the channel and u is the average flow rate in the microchannel. Using this equation, we found that an average flow rate of $\sim 460 \dfrac{\mu l}{min}$ is required in order that the shear stress exerted on the cells in the continuous-flow experiments becomes equal to that we estimate they experience in the acoustofluidic experiments, i.e., $\tau_c \approx \tau_w$.
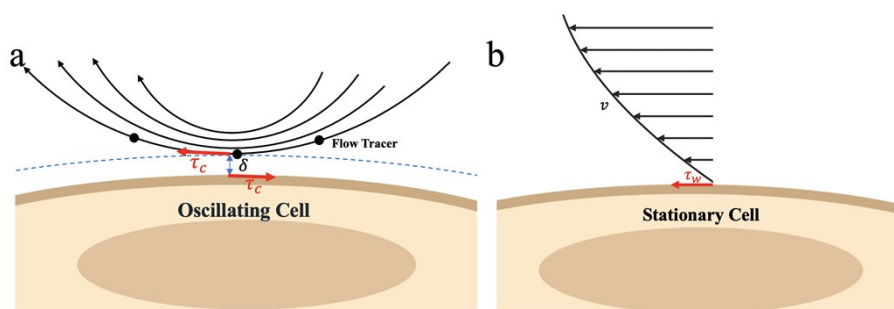
Figure S3. Schematic (not to scale) of the flow profile and the shear stress calculation in the (a) acoustofluidic and (b) continuous-flow experiments. For measuring the maximum microstreaming flow, we used 1-µm flow tracers. The schematic is created with Biorender.com.
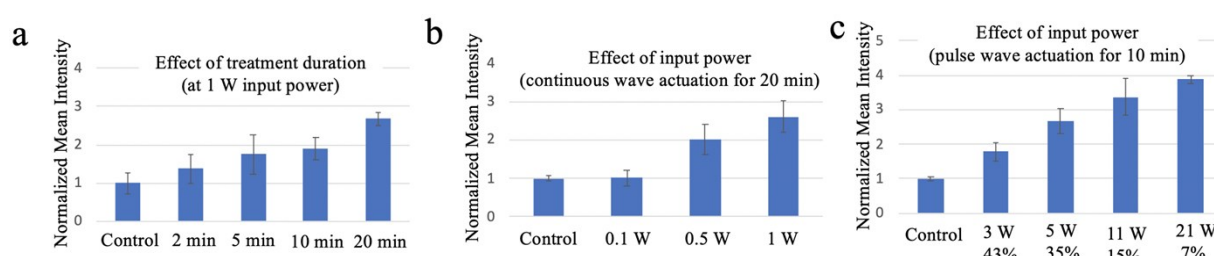
Figure S4. Effect of input power and treatment duration on intracellular delivery. (a) The delivery results for different treatment duration when continuous 1 W input power is applied. (b) Delivery results for the input power in the range of 0.1–1 W and 20 min treatment. (c) Delivery results for different input powers in the range of 3–21 W. For each input power, the duty cycle of the square-waves is set in the range of 7–43% for 10 min treatment duration, to avoid excessive heat generated by the transducer and vibrating PDMS. In all experiments, 3 kDa dextran is used as the cargo material for delivery into MDA-MB-231 cells. The mean intensities are normalized by the values of control experiments. The error bars indicate one standard deviation of three independent experiments (N = 3).
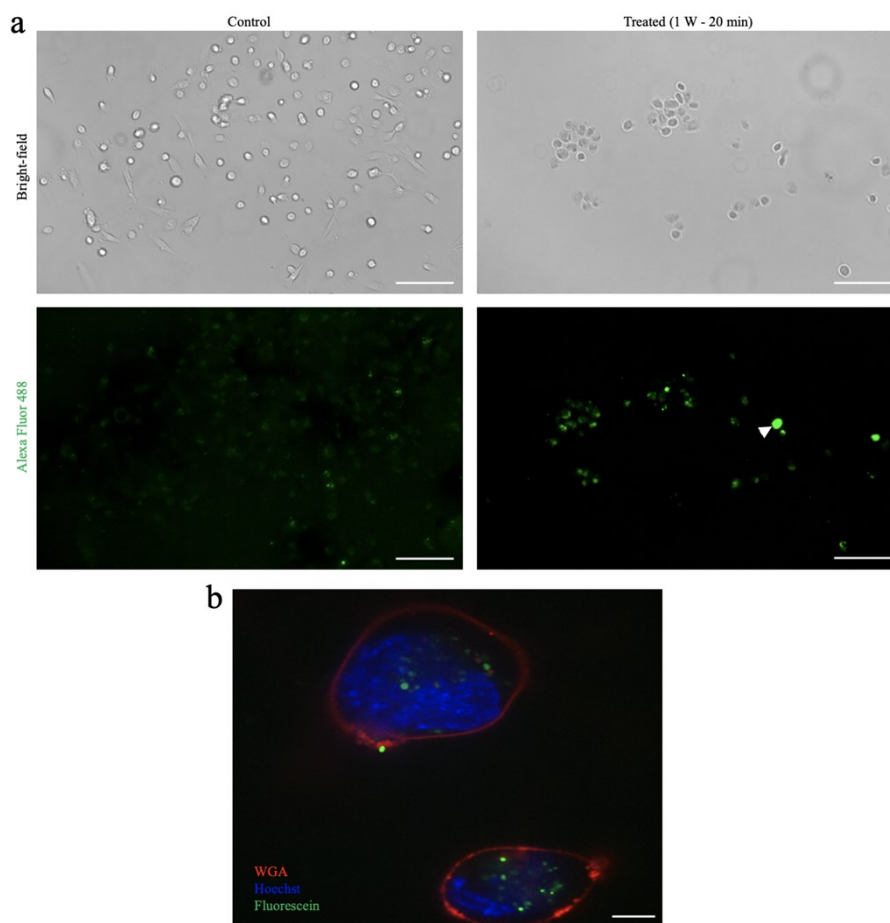
Figure S5. (a) Bright-field and fluorescence images showing the cellular uptake of 3 kDa Alexa 488 dextran in control and treated MDA-MB-231 cells. The white arrowhead points to an individual cell as an example of those receiving cargo material as a result of a potential disruptions to the cell membrane. (b) A confocal image of viable MDA-MB-231 cells exhibiting the uptake of fluorescein-conjugated 500 kDa dextran. Plasma membrane and nucleus of the cells are stained with wheat germ agglutinin (WGA) and Hoechst 33342, respectively. The scale bars represent 100 µm in (a) and 20 µm in (b). For the treatment, a 20 min continuous square-wave at 1 W input power is used.
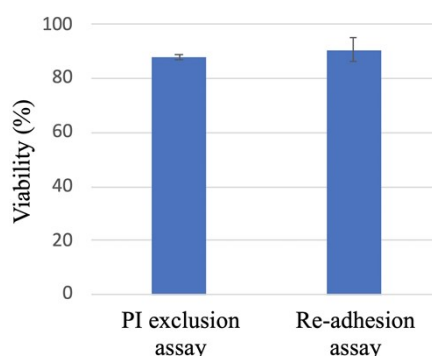
Figure S6. Viability results for when a high-power (i.e., 200 W) actuation pulse is used, which causes the cells to detach. Here, we measure the viability using two different assays: Propidium iodide (PI) exclusion assay and re-adhesion assay. During the detachment, the cell membrane might be compromised, and therefore, might allow the PI to be taken up and thus be counted falsely as dead cells. As a result, we also monitored cells over 16 hr posttreatment to evaluate their re-adhesion. The viability of cells in this case was calculated by dividing the number of re-adhered cells to the total number of cells.
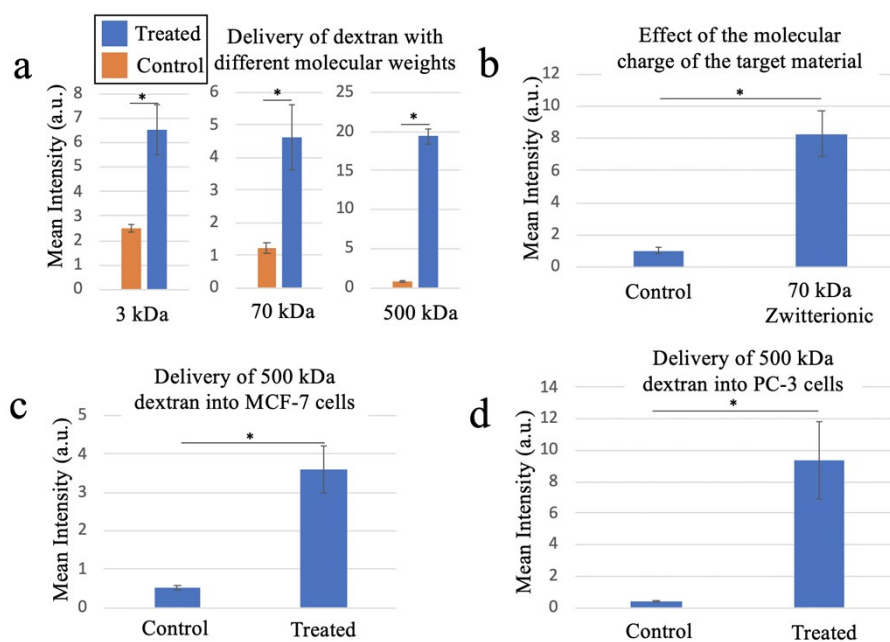
Figure S7. The versatility of intracellular delivery of dextran with various sizes and charges into different cells. Delivery results for dextran (a) with different molecular weights and (b) charges into MDA-MB-231 cells. Delivery results for (c) MCF-7 and (d) PC3 cells. A 20 min continuous square-wave at 1 W input power is used in all experiments. Data show mean values ± one standard deviation, representative of three experiments (* $P < 0.05$ by 2-tailed Student's t-test).
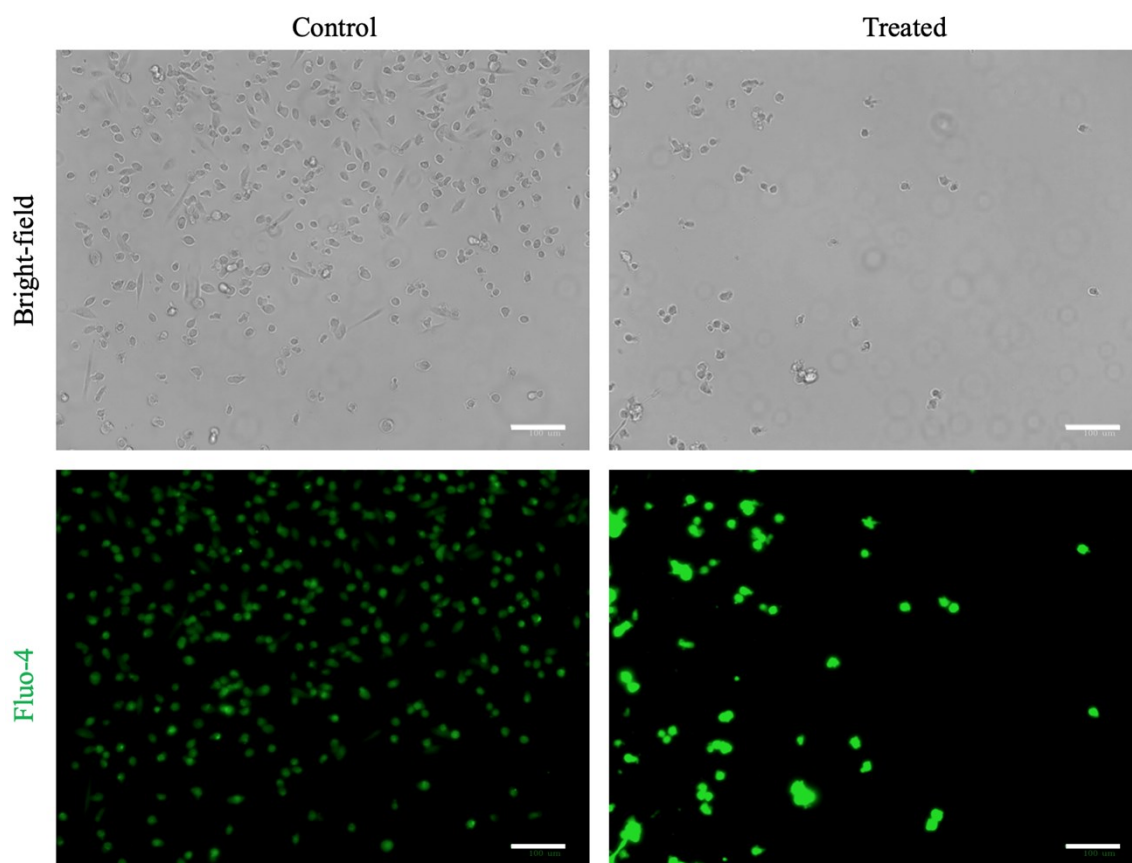
Figure S8. Bright-field and fluorescence images of the control and treated MDA-MB-231 cells. Compared to the control cells, the treated ones show a higher fluorescence intensity of Fluo-4 AM, which is a labelled cell-permeant indicator of Ca^{+2}. The scale bars represent 100 μm.
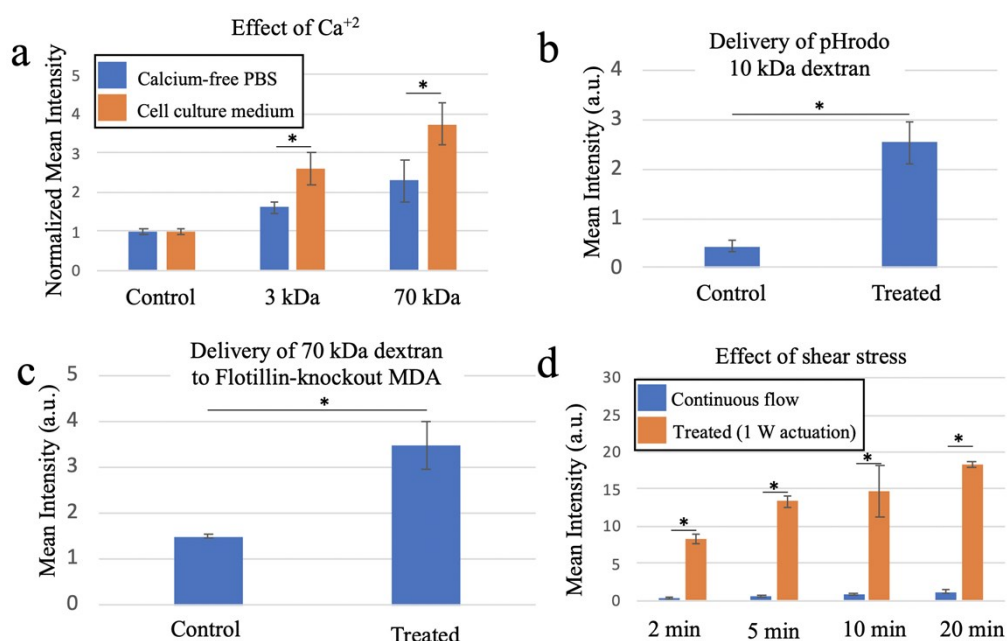
Figure S9. Probing possible mechanisms of delivery. (a) Effect of Ca^{+2} on the delivery of 3 kDa and 70 kDa dextran. (b) Delivery results of pHrodo Green 10 kDa dextran, which fluoresces at low pH values, as an indication of the endosomal pathway role in intracellular delivery. (c) Effect of flotillin-dependent

endocytosis on the uptake of 70 kDa dextran. (d) Effect of exposure to continuous flow (shear stress only), compared to acoustic excitation, on the uptake for different exposure durations. Acoustically actuated cells exhibit significantly higher uptake compared to those exposed to shear stress only. Treatments are conducted on MDA-MB-231 cells using a 20 min continuous square-wave at 1 W input power. The mean intensities in (a) are normalized by the values of control experiments. Data show mean values ± one standard deviation, representative of three experiments (* $P < 0.05$ by 2-tailed Student's t-test).
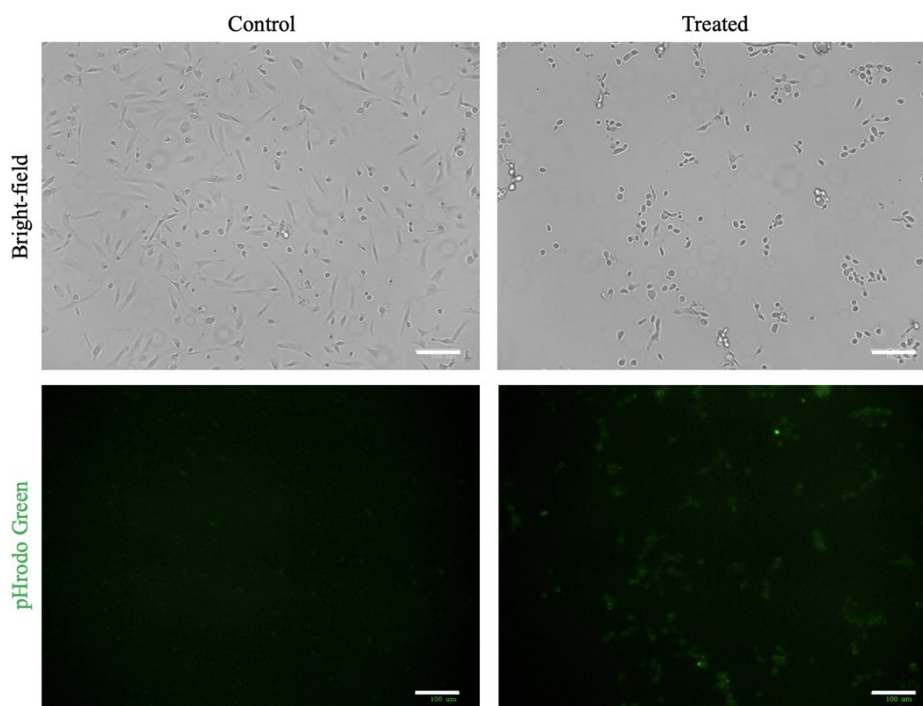
Figure S10. Bright-field and fluorescence images of the control and treated MDA-MB-231 cells. In both control and treatment experiments, the fluorescence images are taken before the pHrodo Green 10 kDa dextran solution is washed out. Compared to the controlled cells, the higher fluorescence intensity of pHrodo Green dextran suggests the formation of more endosomes in the treated cells. The scale bars represent 100 μm.
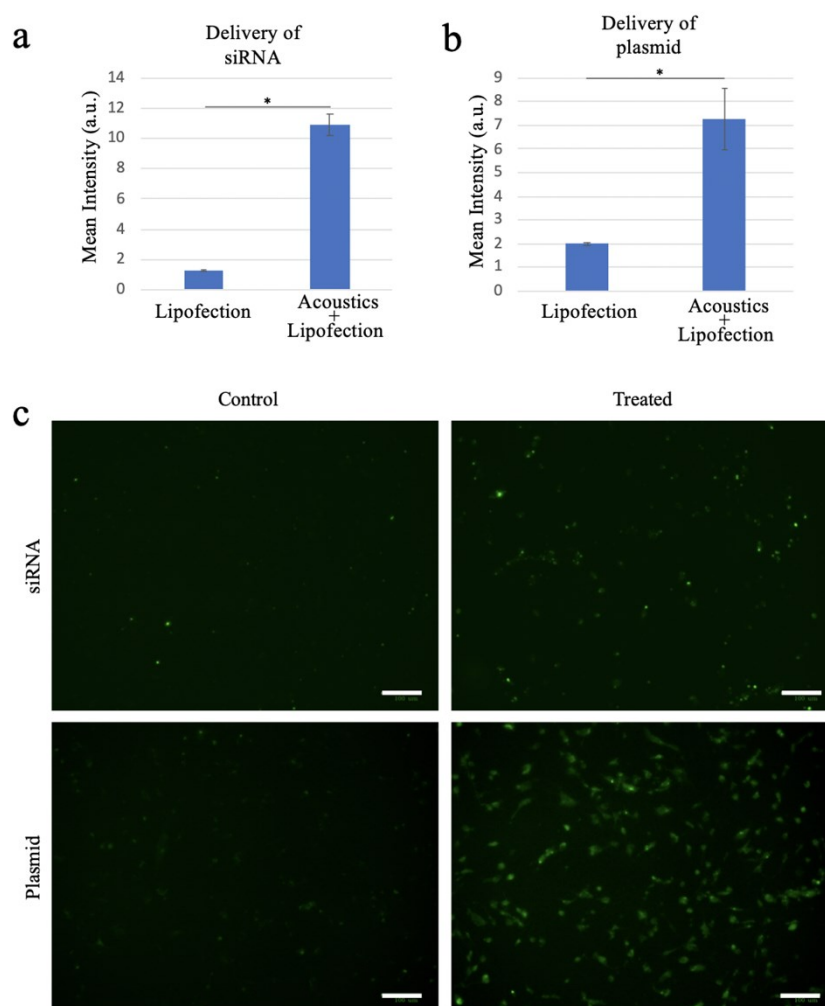
Figure S11. Intracellular delivery of the genetic material. Delivery results of (a) siRNA and (b) plasmid (expression of EGFP). Treatments are conducted on MDA-MB-231 cells using a 20 min continuous square-wave at 1 W input power. Results shown for the control groups are taken from the experiments of conventional transfection with the lipofection duration equal to that of the acoustic treatment experiments. (c) Shows the fluorescence images of the control and treated cells. Data in (a-b) show mean values ± one standard deviation, representative of three experiments (* $P < 0.05$ by 2-tailed Student's t-test). The scale bars in (c) represent 100 µm.

References

1   B. D. M. Meijering, L. J. M. Juffermans, A. Van Wamel, R. H. Henning, I. S. Zuhorn, M. Emmer, A. M. G. Versteilen, W. J. Paulus, W. H. Van Gilst, K. Kooiman, N. De Jong, R. J. P. Musters, L. E. Deelman and O. Kamp, *Circ. Res.*, 2009, **104**, 679–687.

2   A. Sharei, J. Zoldan, A. Adamo, W. Y. Sim, N. Cho, E. Jackson, S. Mao, S. Schneider, M.-J. Han, A. Lytton-Jean, P. A. Basto, S. Jhunjhunwala, J. Lee, D. A. Heller, J. W. Kang, G. C. Hartoularos, K.-S. Kim, D. G. Anderson, R. Langer and K. F. Jensen, *Proc. Natl. Acad. Sci. U. S. A.*, 2013, **110**, 2082–2087.

3   A. Sharei, R. Trifonova, S. Jhunjhunwala, G. C. Hartoularos, A. T. Eyerman, A. Lytton-Jean, M. Angin, S. Sharma, R. Poceviciute, S. Mao, M. Heimann, S. Liu, T. Talkar, O. F. Khan, M. Addo, U. H. Von Andrian, D. G. Anderson, R. Langer, J. Lieberman and K. F. Jensen, *PLoS One*, 2015, **10**, 1–12.

4   J. Wu, *Prog. Biophys. Mol. Biol.*, 2007, 93, 363–373.

5   M. Bahrami, M. M. Yovanovich and J. R. Culham, *J. Fluids Eng. Trans. ASME*, 2006, **128**, 1036–1044.